

Theory on the Stability of the Ferromagnetic Double Layer Structure and on the Peak Structure of the Magneto-Optical Spectra of CeSb

Fumihiko ISHIYAMA* and Osamu SAKAI¹,

Department of Physics, Tohoku University, Sendai 980-8578

¹*Department of Physics, Tokyo Metropolitan University, Hachioji 192-0397*

(Received —————)

We propose the $pf+pd$ mixing model for CeSb to explain the stability of the ferromagnetic double layer structure in the magnetic ordering. The pd mixing causes the saddle type singular points, neighboring the Δ axis, for the bands which gain energy through the pf hybridization with the occupied f state. The peak of the density of states due to this combined effect of the pf mixing and the pd mixing enhances the stability of the double layer structure. The same combined effect also causes the saddle type singular points in the joint density of states of the optical transition. The peak structure of the magneto-optical spectra which has been observed in experiments is explained by the present model.

KEYWORDS: CeSb, magnetic order, double layer structure, optical conductivity, pf mixing model

§1. Introduction

Cerium monopnictides (CeX_p , $X_p=P$, As, Sb, Bi) are semimetals with the NaCl type lattice. Their electronic bands have hole surfaces originated from atomic X_p p states around Γ , and electron surfaces originated from Ce $5d$ states around three equivalent X .¹⁾ In the temperature (T) and the magnetic field (H) diagram,^{2,3)} CeX_p 's show various types of magnetic ordered states. They consist of the ferromagnetic layers which stack antiferromagnetically. Many types of stacking sequences appear in the phase diagram. Among CeX_p 's, $CeSb$ ³⁾ and $CeBi$ ^{4,5)} have the type-IA antiferromagnetic (+ + --) phase with nearly full ($J_z \simeq \pm 5/2$) magnetic moment as the ground state of weak H case. Here '+' denotes the ferromagnetic layer with the magnetic moment parallel to the field, and '-' denotes the layer anti-parallel to the field.

The pair of ferromagnetic layers (+ + or --) is widely observed as a unit of the magnetic structure in CeX_p 's. We call it as the 'double layer structure', hereafter.

The phase diagram of CeSb has been qualitatively reproduced by the ANNNI model.⁶⁻⁸⁾ However, it is not clear how the parameters of the phenomenological model are related to those of the microscopic model.

The origin of the ferromagnetic layer with nearly full moment was explained by the pf mixing model⁹⁻¹⁶⁾ proposed by Kasuya *et al.* The model also succeeded in explaining the origin of the antiferromagnetic stacking of the ferromagnetic layers. However, the stability of the double layer structure with sufficient energy gain has not been obtained.

The pd mixing term between X_p p bands and Ce d bands is neglected in the energy calculation of the original pf mixing model, because the pd mixing effect dis-

appears on the Δ axis where the pf mixing becomes maximum. Later, it was pointed out that the pd mixing term plays important role¹⁷⁻¹⁹⁾ to explain the Fermi surfaces of CeSb in the ferromagnetic phase²⁰⁻²⁵⁾ and + + -- phase.^{25,26)}

In this paper, we employ the pf mixing model including the pd mixing effect, and examine the stability of the double layer structure in CeSb. Hereafter, we call the model as the $pf+pd$ mixing model. It is shown that the p bands, which are pushed up by the occupied f state to gain the pf mixing energy, hybridize through the pd mixing with the d bands around the Δ axis. This combined effect of the pf mixing and the pd mixing causes saddle type singular points neighboring the Δ axis, and substantiates the energy gain due to the pf hybridization. The double layer structure is stabilized by the combined effect.

We also study the magneto-optical spectra of CeSb. Recently, the magneto-optical spectra in various magnetic ordered states have been extensively studied experimentally by Pittini *et al.*²⁷⁾ and by Kimura *et al.*²⁸⁻³⁰⁾ The individual magnetic ordered state shows its own characteristics in the optical conductivity spectra. The spectra will give us fine information on the electronic states in the magnetic ordered states and work as a good probe to study the characteristic band structure of the $pf+pd$ mixing model. The peak structures observed in the experiments are explained by the saddle type singular points in the joint density of states, which are caused by the combined effect of the pf mixing and the pd mixing.

In the next section, we introduce the $pf+pd$ mixing model. In section 3, the stability of the double layer structure is examined. In section 4, the optical conductivity in the magnetic ordered state is calculated. Finally, we summarize the results obtained by the $pf+pd$ mixing model in section 5.

* Contact address: NTT Energy and Environment Systems Laboratories, Tokyo 180-8585

§2. Model

Let us choose the z axis along the magnetic polarization, then the ferromagnetic layer is in the xy plane. We denote the layer which has the polarization parallel to the axis by the sign ‘+’, and the layer which has the polarization anti-parallel to the axis by the sign ‘-’. The magnetic ordering is classified by the stacking sequence of layers along the axis.

We employ the following Hamiltonian,

$$H = H_f + H_p + H_d + H_{pd} + H_{pf}, \quad (2.1)$$

$$H_f = \sum_l \left\{ \sum_{t=\kappa, \nu} \varepsilon_f f_t^\dagger(\mathbf{R}_l) f_t(\mathbf{R}_l) + U_{ff} f_\kappa^\dagger(\mathbf{R}_l) f_\kappa(\mathbf{R}_l) f_\nu^\dagger(\mathbf{R}_l) f_\nu(\mathbf{R}_l) \right\}, \quad (2.2)$$

$$H_p = \sum_{\mathbf{k}} \sum_{t=\kappa, \nu} \varepsilon_p(\mathbf{k}) p_t^\dagger(\mathbf{k}) p_t(\mathbf{k}), \quad (2.3)$$

$$H_d = \sum_{\mathbf{k}} \sum_{s=\alpha, \beta} \varepsilon_d(\mathbf{k}) d_s^\dagger(\mathbf{k}) d_s(\mathbf{k}), \quad (2.4)$$

$$H_{pd} = \sum_{\mathbf{k}} \sum_{s=\alpha, \beta} \sum_{t=\kappa, \nu} V_{pd}(\mathbf{k}, s, t) p_t^\dagger(\mathbf{k}) d_s(\mathbf{k}) + h.c., \quad (2.5)$$

$$H_{pf} = \sum_{\mathbf{k}} \sum_l \sum_{t, t'=\kappa, \nu} V_{pf}(\mathbf{k}, t, t') \times e^{i\mathbf{k} \cdot \mathbf{R}_l} f_t^\dagger(\mathbf{R}_l) p_{t'}(\mathbf{k}) + h.c.. \quad (2.6)$$

Here, H_f stands for the f states, and \mathbf{R}_l denotes site l . The quantities $f_\kappa(\mathbf{R}_l)$ and $f_\nu(\mathbf{R}_l)$ are the annihilation operators of the f electrons at \mathbf{R}_l with κ and ν components of the Γ_8 symmetry, respectively.¹³⁾ These states have large magnetic moment along the z axis, and are considered as the main components of the ferromagnetic layers.^{19, 31)} κ and ν are ascribed to the + layers and the - layers, respectively. ε_f is the f level, and U_{ff} is the f - f Coulomb potential.

H_p stands for the p bands which have hole surfaces around Γ . $p_t(\mathbf{k})$ denotes the annihilation operator of the p band electron with symmetry t . There are six sheets of p bands. Among them, we consider only κ and ν components of the Γ_8 symmetry which mainly mix with κ and ν components of the f states. The remaining two bands of the Γ_8 symmetry (λ and μ) are treated as a reservoir, and the two bands of the Γ_7 symmetry are neglected because they do not have Fermi surface.

H_d stands for the d bands which have electron surfaces around X . $d_s(\mathbf{k})$ denotes the annihilation operator of the d band electron with the xy symmetry and the spin index s . The xy bands mix with the p bands with κ and ν symmetry in the energy region near the Fermi energy, E_F . We retain the xy bands in H_d , and the other d bands (yz and zx) are treated as a reservoir. In the d bands, we use the spin index s (α and β) because the spin-orbit interaction is negligible. H_{pd} and H_{pf} stand for the band mixing terms.

In the Hamiltonian, we have retained only the bands which are mainly affected by the magnetic ordering char-

acterized by the ferromagnetic layers in the xy plane. Therefore the cubic symmetry of the paramagnetic phase is lost at this stage. The Δ -symmetry axis along the z axis is called as the Δ_Z axis, hereafter.

In the phase diagram, there appear layers which are denoted by ‘0’.³⁾ They have small sublattice magnetic moment and are considered as the layers with the Γ_7 symmetry.³¹⁾ In this paper, we assume that the Γ_7 layer is inert for the band structure because the pf mixing is weak for the Γ_7 states.

We introduce Schrieffer-Wolff transformation³²⁾ to avoid treating the f states as the f bands, and to improve the precision of the numerical process in the band energy calculation. With this transformation for the ordered states, the pf mixing term is replaced as the effective p - p term as follows:

$$H'_{pf} = - \sum_{\mathbf{k}} \sum_{t, t', t''=\kappa, \nu} \sum_{n=0}^{N-1} \frac{1}{\varepsilon_f} \times V_{pf}^*(\mathbf{k} + n\Delta\mathbf{k}, t, t') V_{pf}(\mathbf{k}, t, t'') \times \frac{1}{N} \sum_{l=0}^{N-1} n_t(l) e^{-2\pi i \frac{ln}{N}} \times p_{t'}^\dagger(\mathbf{k} + n\Delta\mathbf{k}) p_{t''}(\mathbf{k}), \quad (2.7)$$

with $E_F = 0$ and $\Delta\mathbf{k} = (0, 0, 2\pi/(Na))$. N is the period of the magnetic ordering, and $\Delta\mathbf{k}$ is the basic reciprocal lattice vector corresponding to the period of the magnetic ordering, where $2a$ is the length of the edge of the cube of the fcc lattice. $\Delta\mathbf{k}$ is obtained by choosing primitive translation vectors, one of which represents the magnetic ordering and the other two vectors are $(2a, 0, 0)$ and $(a, a, 0)$ in the xy plane of the fcc lattice. Of course, the wave number vector $\mathbf{k} + n\Delta\mathbf{k}$ should be contained in the first Brillouin zone of the fcc lattice. $n_t(l)$ is the occupation number of t state on the l -th layer in the unit cell of the magnetic ordered state. In eq.(2.7), the terms which are written as the single site energy of the f states are dropped. They are common for κ and ν (and also for the other states of Γ_8). This cubic crystal field splitting term due to the pf mixing should be included when we compare the energy of the phases with various fraction of the Γ_8 states. Since the bases of the bands are restricted, only the terms which satisfy the condition $t = t' = t''$ in eq.(2.7) appear.

The band parameters are fitted so as to reproduce the band structure of LaSb.¹⁾ Table I shows the band pa-

Table I. Band parameters

(eV)	p	d	pd	pf
ε_a	-0.495	2.526	—	—
σ_1	0.256	-0.681	0.766	0.350
π_1	-0.020	0.196	-0.653	-0.245
δ_1	—	0.000	—	—
σ_2	0.087	0.000	—	—
π_2	0.104	0.000	—	—
δ_2	—	0.023	—	—

rameters used in the present calculation. ε_a is the atomic energy levels. σ_1 , π_1 and δ_1 are the two center integral parameters for the nearest neighbor sites. σ_2 , π_2 and δ_2 are the parameters for the next nearest neighbor sites. The next nearest neighbor terms are included to reproduce the band dispersion curve precisely on the Δ_Z axis where the pf mixing becomes maximum. The parameter values of the pd mixing term and the pf mixing term are the ones used in the previous studies.¹²⁾ In later calculation, we control the strength of the pf mixing effect by changing $-1/\varepsilon_f$. Here, ε_f is measured from the Fermi energy of the paramagnetic phase.

The energy of each ordered state is calculated from the density of states (DOS) by the equation

$$E = \int_{-\infty}^{E_F} dE' (D_B(E') + D_R(E')) E'. \quad (2.8)$$

Here, D_B is the DOS of the bands which are treated explicitly in the Hamiltonian, and D_R is the DOS of the reservoir bands. The reservoir is necessary to give the right Fermi energy E_F and the right carrier number. As is shown later, D_B of the phases with double layer structure has a peak splitting structure across the Fermi energy of the paramagnetic phase ($E_F \simeq 0$ eV), and this gives energy gain. Without the reservoir, the Fermi energy rises up above the peak splitting structure, and the energy gain is not obtained. We calculate the DOSs (D_B and D_R) by the tetrahedron method. The calculated energy depends on the number of meshes in the \mathbf{k} -space $N_{\mathbf{k}}$. We extrapolate the energy to the $N_{\mathbf{k}} \rightarrow \infty$ limit as a function of $1/N_{\mathbf{k}}$ from the calculated results of $N_{\mathbf{k}} = 20, 30, 40, 50, 60$, and estimate the extrapolation error ΔE of the energy.

§3. Double Layer Structure

In this section, we calculate the band energy of each magnetic ordered state, and show that the $pf+pd$ mixing model gives the stabilization of the double layer structure.

Figure 1 shows the energy difference between the $++00$ phase and the $+0+0$ phase as a function of ε_f . The energy of the $++00$ phase, which has the double layer structure, becomes lower than that of the $+0+0$ phase in the $pf+pd$ mixing model when the f level ε_f is shallower than -1.5 eV. In contrast, the energy difference between the two is small in the pf mixing model. The magnitude of the energy gain which is obtained by the pf mixing model is comparable to that of the previous work.¹⁵⁾

We have also calculated the energy difference between the $++0000$ phase and the $+00+00$ phase based on the $pf+pd$ mixing model. The former, which has the double layer structure, has lower energy when the pf mixing is strong. The $++000000$ phase has also lower energy than the $+000+000$ phase in the $pf+pd$ mixing model.³³⁾ The magnitude of the relative stability of the $++0000$ phase and the $++000000$ phase is about $1/3$ of that of the $++00$ phase in the range shown in Fig.1. We use the value $\varepsilon_f = -0.7$ eV hereafter to analyze the origin of the stability of the double layer structure.

We note that the $t = \kappa$ component hybridizes only

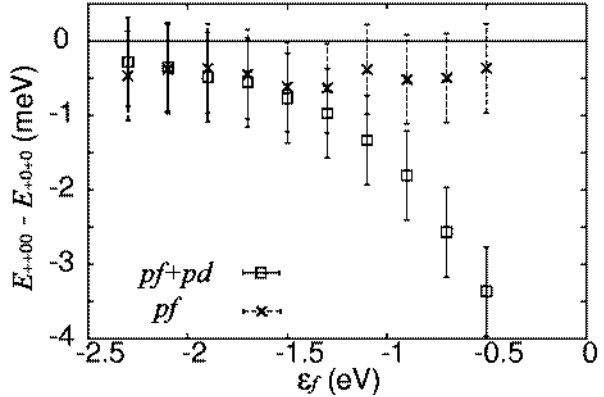


Fig. 1. The energy difference between the $++00$ phase and the $+0+0$ phase $E_{++00} - E_{+0+0}$ as a function of the f level ε_f . \square corresponds to the $pf+pd$ mixing model, and \times corresponds to the pf mixing model. The error bars indicate twice of the extrapolation error ΔE .

with the $s = \alpha$ (up spin) component of the d bands in the present band scheme, because the other components which can weakly hybridize are dropped in eq.(2.1). The κ bands and the α bands do not hybridize with the $t = \nu$ and $s = \beta$ (down spin) components. Therefore, we call the former part as the $+$ -spin bands and the latter as the $-$ -spin bands.

Figure 2 shows the density of states (DOS) of the $+$ -spin bands near E_F . The DOS for the $++00$ phase and that for the $+0+0$ phase are shown. The $+$ -spin bands are mainly modified by the magnetic ordering, and the $-$ -spin bands are not modified because f_ν is not occupied in these phases. The p bands, which are pushed up by

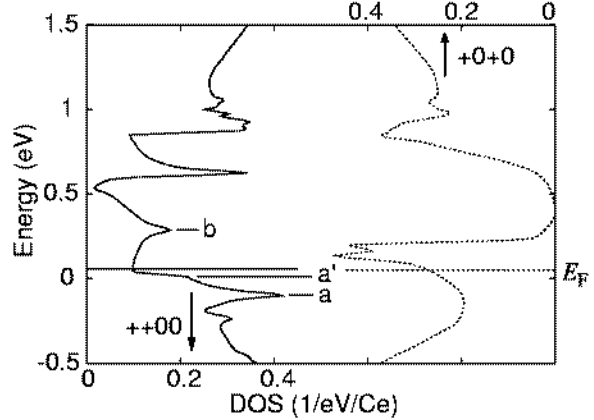


Fig. 2. The DOS of the $+$ -spin bands for the $++00$ phase (solid line) and that for the $+0+0$ phase (broken line). Horizontal lines are E_F for the $++00$ phase (solid line) and that for the $+0+0$ phase (broken line). ε_f is set to -0.7 eV.

the strong pf mixing, strongly mixes with the d bands, and the combined effect causes the peak structure shown in Fig.2. Detailed discussion of the combined effect will be given later. The peak structure in the $+0+0$ phase appears above E_F . Therefore, the combined effect does not contribute to the band energy gain. In contrast, the

peak structure in the $++00$ phase appears below E_F and above E_F (the peaks marked by **a** and **b**). This causes the band energy gain.

Figure 3 shows the band structure of the $+$ -spin bands for the $++00$ phase. A part of the p bands is pushed

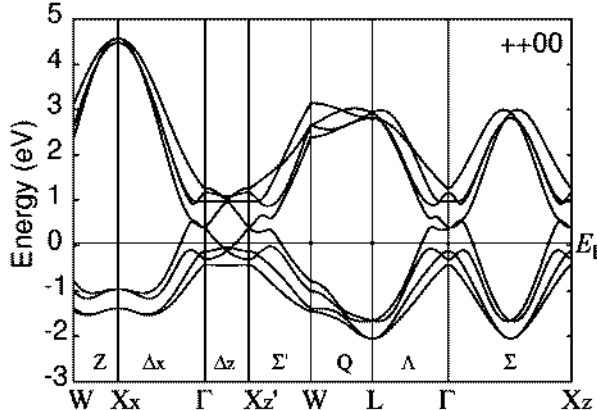


Fig. 3. The band structure of the $+$ -spin bands for the $++00$ phase. These bands correspond to the DOS in Fig.2. X_X corresponds to $(1, 0, 0)$ and X'_Z corresponds to $(0, 0, 1/2)$. The Σ' axis connects $(0, 0, 1/2)$ and $(0, 1/2, 1)$. The other points and axes are the ones of the fcc lattice.

up above E_F on the Δ_Z axis due to the pf mixing with the occupied f states. The p bands have gaps on the Δ_Z axis caused by the ordering of the f states. On this axis, the pf mixing effect is maximum, while the pd mixing disappears due to symmetry. In contrast, the pd mixing term recovers its value steeply when the \mathbf{k} point moves from the Δ_Z axis.³⁴⁾ Since the p bands, which are pushed up by the pf mixing, have energy close to the energy of the d_{xy} bands, the band structure is strongly modified in the vicinity of the Δ_Z axis. This fact is seen in Fig.3. On the axes Δ_X and Σ' , we can see band splitting effect between the p bands and the d bands.

The p bands, which are pushed up above E_F , have small band dispersion along the direction parallel to the Δ_Z axis. Then the pd hybridized bands have approximately cylindric equi-energy surfaces around the Δ_Z axis. This enhances the peak structure of DOS due to the van Hove singularity. We note that the peak **a** in Fig.2 corresponds to the maximum in Fig.3 just below E_F in the Δ_X axis (the 3rd band from the low energy side).

Figure 4 shows the band structure for the $++00$ phase along the $(0, 0, 1/4) - (1, 0, 1/4)$ axis, which is calculated by the $pf+pd$ mixing model. Figure 5 shows one calculated by the pf mixing model. The energies of bands in both cases are identical at $(0, 0, 1/4)$, because the pd mixing disappears due to symmetry. When the point moves to the $(1, 0, 1/4)$ direction, the band splitting due to the pd mixing is seen in Fig.4. The maximum marked by **a'** in Fig.4 corresponds to the shoulder marked by **a'** in Fig.2, and the maximum marked by **b** in Fig.4 corresponds to the peak marked by **b** in Fig.2. We note that the point **a'** has maximum type singular point, and the point **b** has the saddle type singular point.

We note that the DOS of the pf mixing model does

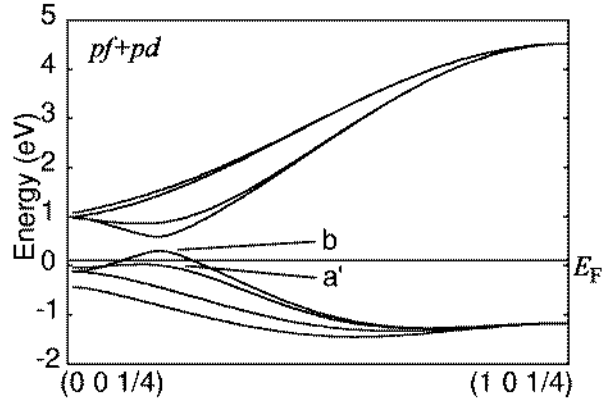


Fig. 4. The band structure for the $++00$ phase along the $(0, 0, 1/4) - (1, 0, 1/4)$ axis in the $pf+pd$ mixing model.

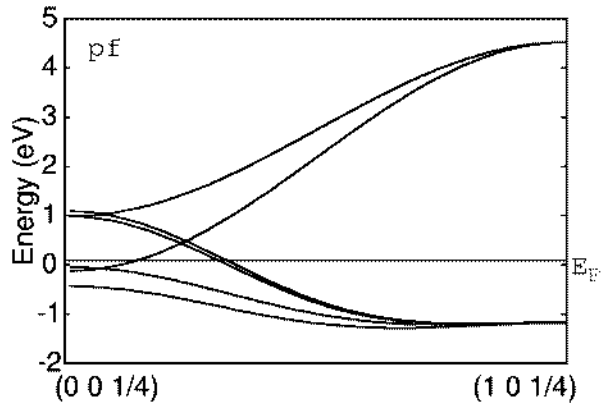


Fig. 5. The band structure for the $++00$ phase along the $(0, 0, 1/4) - (1, 0, 1/4)$ axis in the pf mixing model.

not have fine structure, because of the absence of the pd mixing term. The gain of the band energy due to the combined effect of the pf mixing and the pd mixing around the Δ_Z axis is important to stabilize the double layer structure.

Let us consider the origin of the relative stability between the $++00$ phase and the $+0+0$ phase. The latter phase has the period characterized by the wave number vector $(0, 0, 1)$. At the point where the main band gap is formed, the d band has energy higher than the Fermi energy of the paramagnetic phase. Therefore, the main band repulsion due to the combined effect occurs rather higher energy region. On the other hand, the $++00$ phase is characterized by the wave number vector $(0, 0, 1/2)$. The gap is formed near the Fermi surface of the d_{xy} bands. When we remove the reservoir from the present model, E_F locates just above **b** in Fig.4, and the stability of the $+0+0$ phase is relatively enhanced.

Figure 6 shows the magnetic phase diagram under the field with the parameter $\varepsilon_f = -0.7$ eV. As noted previously, the crystal field splitting between the Γ_8 states and the Γ_7 states,

$$E_{CEF} = E_{\Gamma_8} - E_{\Gamma_7} \quad (3.1)$$

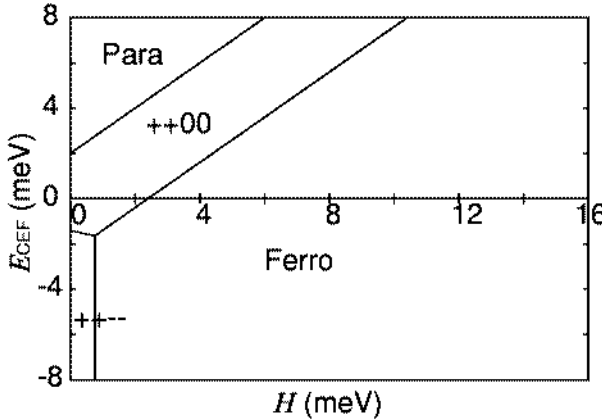


Fig. 6. The magnetic phase diagram with the f level $\varepsilon_f = -0.7$ eV. The transverse axis is the field H , and the ordinate axis is the crystal field splitting E_{CEF} between the Γ_7 layer and the Γ_8 layer ($E_{\Gamma_8} - E_{\Gamma_7}$). ‘Para’ means the Γ_7 phase. The energy of the phases with period-1,2,4 are compared in this figure.

is a free parameter of the present model. The energy difference between the ordered states with different fraction of the Γ_8 layer depends on the quantity E_{CEF} . At the same time, the energy gain from the Zeeman interaction is proportional to the ferromagnetic moment of the phase. We have calculated the energy of each phase assuming following equation

$$E = E_{\text{band}} + (n_+ + n_-)E_{\text{CEF}} - (n_+ - n_-)H. \quad (3.2)$$

Here, n_+ and n_- are the fraction of the + layers and the - layers, respectively. The Γ_7 layers are assumed as non-magnetic layers for simplicity.

When the energy of the Γ_8 layer is enough lower than that of the Γ_7 layer ($E_{\text{CEF}} < -1.4$ meV in Fig.6), the $++--$ phase becomes the ground state in the $H = 0$ case. This phase may correspond to the type-IA phase of CeSb. The phase turns into the ferromagnetic phase in the present calculation, when the field is increased. The boundary between the $++--$ phase and the ferromagnetic phase is about 6 T in the present calculation, and is comparable to the experimental magnitude 4 T.³⁾ In the calculation of the Zeeman energy, the g -value of the Γ_8 states is included as $H \leftarrow g_J \mu_B H$ with $g_J = 6/7$.

When the energy of the Γ_7 layer (*i.e.* the paramagnetic layer in the present model) is enough lower than that of the Γ_8 layer ($E_{\text{CEF}} > 2$ meV in Fig.6), the Γ_7 phase (0000) becomes the ground state. This phase turns into the ferromagnetic phase by way of the $++00$ phase as the field increases.

The phase transition with the parameter $E_{\text{CEF}} > 2$ meV will mimic that of CeP, whose ground state is the antiferromagnetic Γ_7 phase. In CeP, the phase successively turns into the states which have large fraction of double Γ_8 layers when the field is increased.²⁾

§4. Optical Conductivity Spectra

In this section, we calculate optical conductivity spectra based on the $pf+pd$ mixing model. The optical conductivity spectra for the ± 1 circular light, $\sigma_{\pm}(E)$, of the

magnetic ordered states are given by the following expression,

$$\begin{aligned} \sigma_{\pm}(E) & \propto \int_{\text{BZ}} d^3k \sum_{i,j,n,s,t} \sum_{E_i(\mathbf{k}) < E_F < E_j(\mathbf{k})} \delta(E_j(\mathbf{k}) - E_i(\mathbf{k}) - E) \\ & \times | \langle a_j(\mathbf{k}) | d_s(\mathbf{k} + n\Delta\mathbf{k}) \rangle \langle p_t(\mathbf{k} + n\Delta\mathbf{k}) | a_i(\mathbf{k}) \rangle |^2 \\ & \times w(\mathbf{k} + n\Delta\mathbf{k}) c_{\pm}^{p \rightarrow d}(s, t) \\ & + \int_{\text{BZ}} d^3k \sum_{i,j,n,s,t} \sum_{E_i(\mathbf{k}) < E_F < E_j(\mathbf{k})} \delta(E_j(\mathbf{k}) - E_i(\mathbf{k}) - E) \\ & \times | \langle a_j(\mathbf{k}) | p_t(\mathbf{k} + n\Delta\mathbf{k}) \rangle \langle d_s(\mathbf{k} + n\Delta\mathbf{k}) | a_i(\mathbf{k}) \rangle |^2 \\ & \times w(\mathbf{k} + n\Delta\mathbf{k}) c_{\pm}^{d \rightarrow p}(s, t), \end{aligned} \quad (4.1)$$

$$\Delta\mathbf{k} = (0, 0, \frac{2\pi}{Na}). \quad (4.2)$$

where $a_j(\mathbf{k})$ stands for the diagonalized band with the band index j , and BZ means the integration in the Brillouin zone. $w(\mathbf{k} + n\Delta\mathbf{k})$ stands for the \mathbf{k} dependence of the optical transition probability. The term $w(\mathbf{k} + n\Delta\mathbf{k})$ is proportional to $(\cos k_x + \cos k_y)^2$, since the present $p \leftrightarrow d$ transition is the inter-site process. However, we assume the term as constant, because the saddle type singular points which correspond to the peak structure of the spectra are located neighboring the Δ_Z axis where $k_x \simeq 0$ and $k_y \simeq 0$. s and t represent the indices of the d states (α and β) and the p states (κ and ν) respectively. The terms $c_{\pm}^{p \rightarrow d}(s, t)$ and $c_{\pm}^{d \rightarrow p}(s, t)$ stand for the selection rule of the optical transition. They have 1 for $c_+^{p \rightarrow d}(\alpha, \kappa)$, $c_+^{d \rightarrow p}(\beta, \nu)$, $c_-^{p \rightarrow d}(\beta, \nu)$, $c_-^{d \rightarrow p}(\alpha, \kappa)$, and 0 for the other combinations of s and t . We note that the optical transition matrix appears only between p_{κ} and d_{α} states, or between p_{ν} and d_{β} states in the present simplified model. At the same time, the + spin bands (which consists of p_{κ} and d_{α}) do not hybridize with the - spin bands (p_{ν} and d_{β}). By the facts, the optical conductivity is separated into the $p \rightarrow d$ components and the $d \rightarrow p$ components as expressed in eq.(4.1).

Figure 7 shows the calculated optical conductivity spectra for the ferromagnetic phase. $\sigma_{-}(E)$ for various ε_f cases are shown in the figure. When the pf mixing is large enough, one of the p bands is pushed up above E_F around X_Z . Then, the $d \rightarrow p$ transition around X_Z comes to be possible, and the transition contributes to $\sigma_{-}(E)$. The band in the ferromagnetic phase has a saddle type singular point of the joint density of states at X_Z , and the peak structure, which corresponds to the transition around this point, appears in $\sigma_{-}(E)$. On the other hand, $\sigma_{+}(E)$ is essentially equivalent to that of the paramagnetic phase consistently with the experimental results by Kimura *et al.*^{28,29)}

The energy of the peak E_{peak} in Fig.7 becomes higher as the strength of the pf mixing effect, which is proportional to $-1/\varepsilon_f$, becomes larger. At the same time, the strength of the peak increases as the intensity of the pf mixing effect increases, because the \mathbf{k} -space which contributes to the peak becomes wider.

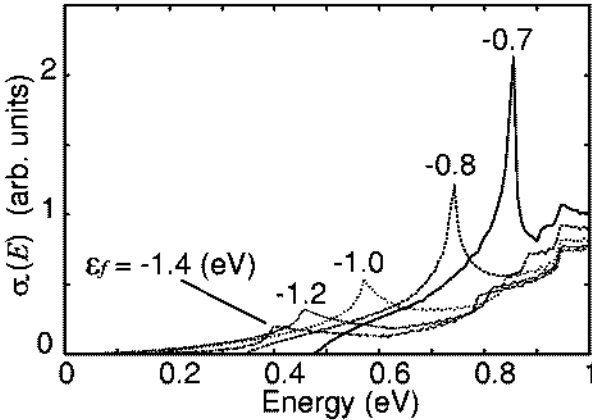


Fig. 7. The optical conductivity spectra $\sigma_-(E)$ for the ferromagnetic phase. The spectra for $\varepsilon_f = -1.4, -1.2, -1.0, -0.8, -0.7$ eV are shown. The intensity of the pf mixing is proportional to $-1/\varepsilon_f$.

Figure 8 shows the relation between the energy of the peak E_{peak} of the ferromagnetic phase and $-1/\varepsilon_f$. The marks '+' in the figure are roughly on the line of

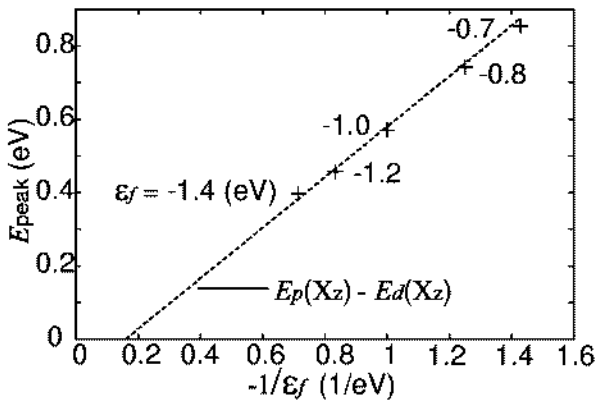


Fig. 8. The energy of the peak E_{peak} of the ferromagnetic phase versus the strength of the pf mixing effect ($-1/\varepsilon_f$). The peak energy is plotted by '+' sign. The broken line represents the energy difference at X_Z between the p band E_p and the d band E_d .

$E_p(X_Z) - E_d(X_Z)$, which is the energy difference between the p band and the d band at X_Z .

Using the relation between the energy of the peak and $-1/\varepsilon_f$, we can determine $-1/\varepsilon_f$ from the experimental results.²⁸⁾ We obtain the value of the f level as $\varepsilon_f = -1.35$ eV from Fig.8, where the peak appears at 0.4 eV. In later calculation of the optical conductivity, we employ this value. In this case, the energy difference in Fig.1 becomes about half of that of the $\varepsilon_f = -0.7$ eV case, and this case also holds the condition of the relative stability of the double layer structure. The value of ε_f depends on the magnitude of the pf hybridization matrix element.³⁵⁾ On the other hand, the energy of the peak directly corresponds to the band energy difference $E_p(X_Z) - E_d(X_Z)$. Therefore, the present choice means that the later calculation is carried out based on the band

parameters which give the band energy difference 0.4 eV in the ferromagnetic phase at X_Z . When we use this readjustment, the calculated spectral change due to the change of the magnetic ordering will scarcely depend on the detailed choice of the band parameters.

We note that the transition around X_Z becomes a maximum type singular point in the pf mixing model. Therefore, we do not have peak structure at this energy, if the pd mixing is neglected. We also note that the reservoir bands are not modified by magnetic ordering, and their optical conductivity spectra are equivalent to those of the paramagnetic phase. The low energy peak structure which appears in the ordered states will be scarcely affected by the contribution from the transitions among the reservoir bands.

Figure 9 shows the calculated optical conductivity spectra for the $++-$ phase with $\varepsilon_f = -1.35$ eV. Both

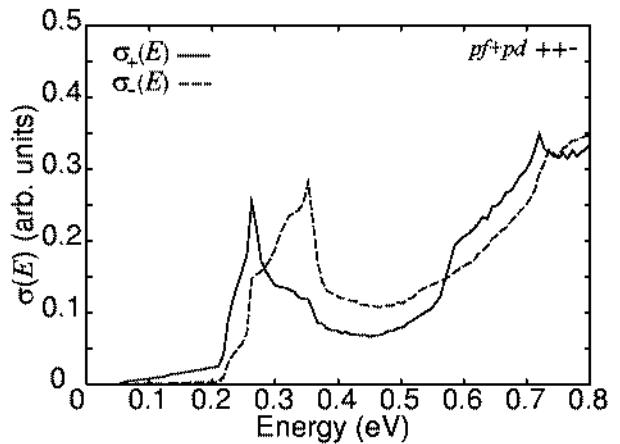


Fig. 9. The optical conductivity spectra for the $++-$ phase.

$\sigma_+(E)$ and $\sigma_-(E)$ have a peak and a shoulder structure which are located at 0.26 eV and at 0.37 eV. The peaks mainly consist of $d \rightarrow p$ transition, and the shoulders mainly consist of $p \rightarrow d$ transition. Both the peaks and the shoulders have the lower energy than the energy of the peak of the ferromagnetic phase. These behaviors are consistent with the observation.³⁰⁾

In the $++-$ phase, the pf mixing pushes up both the $+$ -spin bands and the $-$ -spin bands, and the pd band repulsion makes saddle type singular points which correspond to the structure in Fig.9. In contrast to the peak structure of the ferromagnetic phase, the transition around X_Z does not correspond to the structure.

Figure 10 shows the contour map of the interband transition energy for the $++-$ phase in the \mathbf{k} -space. This map has approximately axial symmetry around the Δ'_Z axis. The peak of $\sigma_+(E)$ and the shoulder of $\sigma_-(E)$ at 0.26 eV in Fig.9 correspond to the saddle type singular point shown by 'x' in Fig.10(a). The former corresponds to the $d \rightarrow p$ transition around the point, and the latter corresponds to the $p \rightarrow d$ transition around the same point. The peak of $\sigma_-(E)$ at 0.37 eV in Fig.9 corresponds to the $d \rightarrow p$ transition around the saddle type singular point shown by 'x' in Fig.10(b), and the shoulder of $\sigma_+(E)$ corresponds to the $p \rightarrow d$ transition

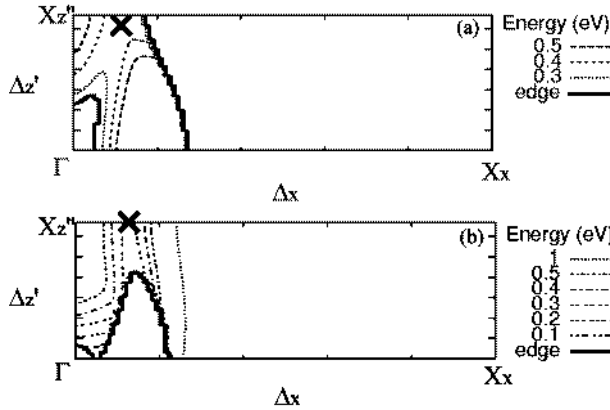


Fig. 10. The equi-energy contour map for the optical transition in the $++-$ phase. The transition of the $+$ -spin bands shown in (a) contributes mainly to the peak at 0.26 eV of $\sigma_+(E)$ and the transition of the $--$ -spin bands shown in (b) contributes mainly to the peak at 0.37 eV of $\sigma_-(E)$. Both peaks correspond to the transition from maxima just below E_F to minima just above E_F near X on the Σ' axis in Fig.10 of ref.30. The equi-energy contours of $E = 0.3, 0.4, 0.5$ eV (a) and those of $E = 0.1, 0.2, 0.3, 0.4, 0.5, 1.0$ eV (b) are plotted. The region where the optical transition does not occur is closed by the contour named ‘edge’. X''_Z is $(0, 0, 1/3)$, and the Δ'_Z axis connects Γ and X''_Z . The saddle type singular points are marked by ‘ \times ’ in the figures.

around the same point.

In Fig.11, we show the optical conductivity spectra for the $++-$ phase calculated by neglecting the pd mixing term (i.e. the pf mixing model). There appears low energy transitions, caused partly by the Brillouin zone folding effect. This case does not have peak structure. That is, the peaks of the optical conductivity spectra

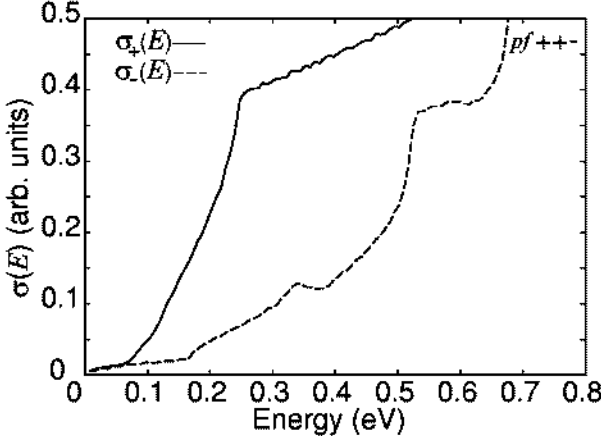


Fig. 11. The optical conductivity spectra for the $++-$ phase of the pf mixing model.

originate from the saddle type singular points caused by the combined effect of the pf mixing and the pd mixing effect.

Figure 12 shows the optical conductivity spectra for the $+0-$ phase with $\varepsilon_f = -1.35$ eV. $\sigma_+(E)$ and $\sigma_-(E)$ are identical, and they have a peak at 0.26 eV. The peak structure in the $+0-$ phase and the structure of $\sigma_+(E)$ in the $++-$ phase shown in Fig.9 have the same energy.

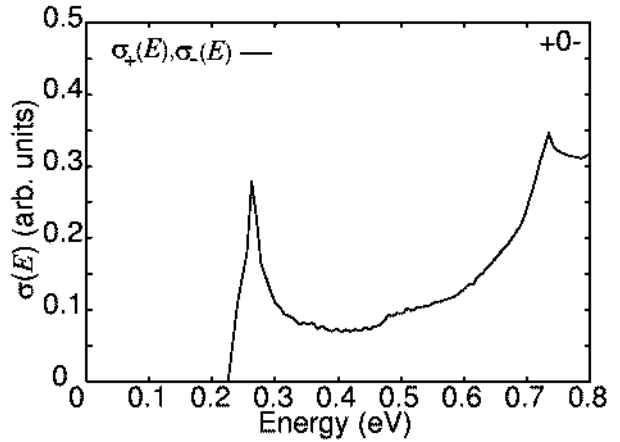


Fig. 12. The optical conductivity spectra for the $+0-$ phase. $\sigma_+(E)$ and $\sigma_-(E)$ have the same spectrum.

It is because the $--$ -spin bands in the $+0-$ phase are identical to those in the $++-$ phase. The difference is on the centroid of the peak, which is shifted to higher energy side in the $++-$ phase than that of the $+0-$ phase due to the contribution from the $+$ -spin bands. The experimental result of the spectra for this phase has not been reported. We expect that the features shown in the figure will be observed.

Figure 13 shows the optical conductivity spectra for the $++00$ phase with $\varepsilon_f = -1.35$ eV. There appears a

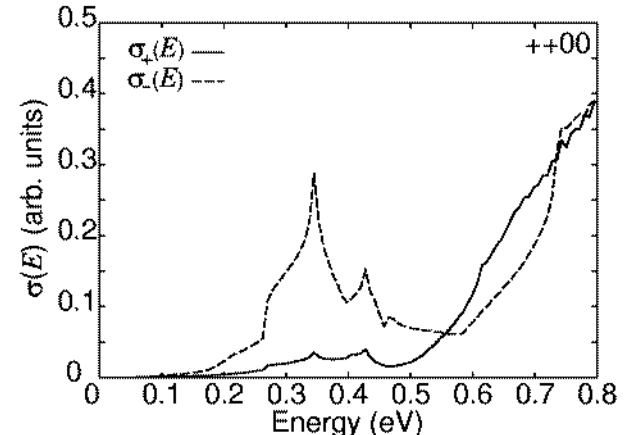


Fig. 13. The optical conductivity spectra for the $++00$ phase.

double peak structure, and both the peaks at 0.35 eV and at 0.43 eV in $\sigma_-(E)$ consist of the $d \rightarrow p$ transition. $\sigma_+(E)$ has the structure corresponding to that in $\sigma_-(E)$ with weak intensity. These results are consistent with the observation.³⁰⁾

In Fig.14, we indicate the saddle type singular points neighboring the Δ'_Z axis which correspond to the peaks of $\sigma_-(E)$ shown in Fig.13. Similarly to the interband transition structure of the $++-$ phase, the dispersion of the transition energy is small in the direction parallel to the Δ'_Z axis around the saddle type singular points, and the cylindrical equi-energy region appears in the $++00$ phase.

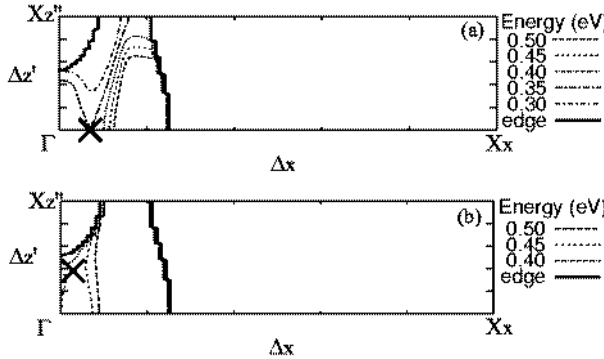


Fig. 14. The equi-energy contour map for the optical transition in the $++00$ phase. Upper figure (a), for which there appears the peak at 0.35 eV, corresponds to the transition from the third lowest band to the fourth lowest band shown in Fig.3, and the lower figure (b), for which there appears the peak at 0.43 eV, corresponds to that from the second lowest band to the fourth lowest band shown in Fig.3. X_Z'' is $(0, 0, 1/4)$, and the Δ_Z' axis connects Γ and X_Z'' . The saddle type singular points are marked by 'x' in the figures. The equi-energy contours of $E = 0.3, 0.35, 0.4, 0.45, 0.5$ eV (a) and those of $E = 0.4, 0.45, 0.5$ eV (b) are plotted. The region where the optical transition does not occur is closed by the contour named 'edge'.

§5. Summary and Discussion

We have demonstrated that the combined effect of the pf mixing and the pd mixing is important to stabilize the double layer structure which is widely observed in the magnetic phase diagram of CeSb. A part of the p bands is pushed up along the Δ_Z axis by the pf mixing with occupied f state. These p bands strongly mix with 5d bands around the Δ_Z axis through the pd hybridization. This causes several bands which have saddle type singular points neighboring the axis. The energy gain due to the pf mixing is substantiated by the pd hybridized bands. The same bands give the saddle type singular points of the joint density of states of the optical transition in the magnetic ordered states. Characteristics of the magneto-optical spectra for various phases of CeSb are reproduced by the calculation.

The energy of the peak structure of the optical conductivity in the ferromagnetic state corresponds to the excitation energy between the pushed up p state and the d state at X_Z . Therefore the peak structure in the ferromagnetic phase of $\text{La}_x\text{Ce}_{1-x}\text{Sb}$ is expected to shift to low energy side as x becomes large, because the pf mixing effect decreases. The peak intensity will also decrease. The situation similar to that shown in Fig.7 will be shown.

In the present paper, we have employed the simplified model to carry out numerical calculation with sufficient accuracy for the band energy of various magnetic phases. The same simplified model accounts the characteristics of the magneto-optical spectra of each magnetic phase. However, the bands treated as the reservoir will also contribute to the spectra in various way. For example, the transition between the reservoir and the states which are modified strongly by the magnetic ordering will be also affected. Such transition terms are not considered in the

present model. Further studies including total bands are necessary in quantitative analysis of the magneto-optical spectra.

Recently, Iwasa *et al.* have proven by the fine X-ray diffraction experiment that the 'paramagnetic layer' consists of the Γ_7 states.³⁶⁾ The present model ascribing the paramagnetic layer as the Γ_7 states will be justified. We have treated the layer as the inert state in the band calculation. In the strict sense, the Γ_7 states have hybridization term with the band states. However, it is not large for the states near the Fermi energy. The essential features of the present result will not be modified even when we include the hybridization term of the Γ_7 states. We expect that the Kondo effect for the paramagnetic state³⁷⁾ will not be so important.

We have shown the stability of the double layer structure on the basis of the band calculation assuming the long range periodicity. The states which include the double layer structure seems to be more stable than the states with isolated layers even when we consider the periodicity of eight layers.³³⁾ Therefore, the explanation of the stability of the double layer structure on the basis of the local electronic structure, in some sense, is desirable. In the experiments on CeP, we observe phases which have very long periodicity with a small number of double layer in the sea of the paramagnetic state.²⁾ Such a study on the isolated double layer is retained in the future. Nevertheless, we note that, in the short periodicity cases, the present band calculation picture will be applicable.

Acknowledgement

The authors would like to thank K. Ueda for encouraging discussions, S. Kimura for comments on experiments, Y. Kuramoto for valuable comments, and H. Harima, Y. Shimizu and Y. Kaneta for supporting numerical calculation. Numerical calculation was partly performed in the Computer Center of Tohoku University, the Supercomputer Center of Institute for Solid State Physics (University of Tokyo) and The Institute of Scientific and Industrial Research (Osaka University).

- 1) A. Hasegawa: J. Phys. Soc. Jpn. **54** (1985) 677.
- 2) M. Kohgi, K. Iwasa and T. Osakabe: Physica B **281&282** (2000) 417.
- 3) J. Rossat-Mignod, J. M. Effantin, P. Burlet, T. Chatopadhyay, L. P. Regnault, H. Bartholin, C. Vettier, O. Vogt, D. Ravot and J. C. Achard: J. Magn. Magn. Mater. **52** (1985) 111.
- 4) H. Bartholin, P. Burlet, S. Quezel, J. Rossat-Mignod and O. Vogt: J. de Physique **40** (1979) C5-130.
- 5) J. Rossat-Mignod, P. Burlet, S. Quezel, J. M. Effantin, D. Delacote, H. Bartholin, O. Vogt and D. Ravot: J. Magn. Magn. Mater. **31-34** (1983) 398.
- 6) J. von Boehm and P. Bak: Phys. Rev. Lett. **42** (1979) 122.
- 7) P. Bak and J. von Boehm: Phys. Rev. B **21** (1980) 5297.
- 8) T. Kasuya, Y. S. Kwon, T. Suzuki, K. Nakanishi, F. Ishiyama and K. Takegahara: J. Magn. Magn. Mater. **90&91** (1990) 389.
- 9) K. Kasuya, K. Takegahara, Y. Aoki, T. Suzuki, S. Kunii, M. Sera, N. Sato, T. Fujita, T. Goto, A. Tamaki and T. Komatsubara: Valence Instabilities ed. by P. Wachter and H. Boppert (1982) 359.

- 10) K. Takegahara, H. Takahashi, A. Yanase and T. Kasuya: Solid State Commun. **39** (1981) 857.
- 11) H. Takahashi and T. Kasuya: J. Phys. C: Solid State Phys. **18** (1985) 2697.
- 12) H. Takahashi and T. Kasuya: J. Phys. C: Solid State Phys. **18** (1985) 2709.
- 13) H. Takahashi and T. Kasuya: J. Phys. C: Solid State Phys. **18** (1985) 2721.
- 14) H. Takahashi and T. Kasuya: J. Phys. C: Solid State Phys. **18** (1985) 2731.
- 15) H. Takahashi and T. Kasuya: J. Phys. C: Solid State Phys. **18** (1985) 2745.
- 16) H. Takahashi and T. Kasuya: J. Phys. C: Solid State Phys. **18** (1985) 2755.
- 17) O. Sakai, M. Takeshige, H. Harima, K. Otaki and T. Kasuya: J. Magn. Magn. Mater. **52** (1985) 18.
- 18) O. Sakai, Y. Kaneta and T. Kasuya: Jpn. J. Appl. Phys. **26** (1987) Suppl. 26-3.
- 19) Y. Kaneta, S. Iwata, T. Kasuya and O. Sakai: J. Phys. Soc. Jpn. **69** (2000) 2559.
- 20) H. Kitazawa: J. Magn. Magn. Mater. **76&77** (1988) 40.
- 21) H. Aoki, G.W. Crabtree, W. Joss and F. Hulliger: J. Magn. Magn. Mater. **52** (1985) 389.
- 22) H. Aoki, G.W. Crabtree, W. Joss and F. Hulliger: J. Magn. Magn. Mater. **97** (1991) 169.
- 23) H. Aoki and G. W. Crabtree: J. Appl. Phys. **57** (1985) 3033.
- 24) R. Settai, T. Goto, S. Sakatsume, Y.S. Kwon, T. Suzuki and T. Kasuya: Physica B **186-188** (1993) 176.
- 25) R. Settai, T. Goto, S. Sakatsume, Y.S. Kwon, T. Suzuki, Y. Kaneta and O. Sakai: J. Phys. Soc. Jpn. **63** (1994) 3026.
- 26) R. Settai, H. Aoki, M. Takashita, T. Terashima, Y. Haga, T. Suzuki, Y. Onuki and T. Goto: Physica B **216** (1996) 310.
- 27) R. Pittini, J. Schoenes, F. Hulliger and P. Wachter: Phys. Rev. Lett. **76** (1996) 3428.
- 28) S. Kimura, H. Kitazawa, G. Kido and T. Suzuki: J. Phys. Soc. Jpn. **69** (2000) 647.
- 29) S. Kimura, H. Kitazawa, G. Kido and T. Suzuki: Physica B **281&282** (2000) 449.
- 30) S. Kimura, M. Okuno, H. Iwata, H. Kitazawa, G. Kido, F. Ishiyama and O. Sakai: J. Phys. Soc. Jpn. **71** (2002) 2200.
- 31) K. Iwasa, Y. Arakaki, M. Kohgi, and T. Suzuki: J. Phys. Soc. Jpn. **68** (1999) 2498.
- 32) J. R. Schrieffer and P. A. Wolff: Phys. Rev. **149** (1966) 491.
- 33) F. Ishiyama and O. Sakai: J. Phys. Soc. Jpn. Suppl. **71** (2002) 294.
- 34) T. Kasuya, Y. Kaneta and O. Sakai: J. Phys. Soc. Jpn **62** (1993) 411.
- 35) O. Sakai, H. Takahashi, M. Takeshige and T. Kasuya: Solid State Commun. **52** (1984) 997.
- 36) K. Iwasa, Y. Araki, M. Kohgi and T. Suzuki: Physica B **281&282** (2000) 437.
- 37) G. Martinez, J.R. Iglesias, C. Lacroix and B. Coqblin: Physica B **281&282** (2000) 440.